Surface wave modelling and near surface characterization background

Andrew Mills, Raul Cova and Kris Innanen

ABSTRACT

Commonly, ground roll "noise" is removed from seismic data, and discarded. While inconvenient for reflection surveying, this apparent noise contains valuable information about the near surface. In this paper, near surface velocity and density models are constructed, and used to model elastic wave propagation of Rayleigh waves through the near surface. Existing near surface characterization techniques are briefly summarized, and used as the basis for this project. Through increasing the complexity or the near surface, issues or shortcomings in existing methods arise in Rayleigh wave dispersion analysis. These issues are identified, and methods of overcoming them are proposed.

INTRODUCTION

In land seismic exploration, where both source and receiver are at the surface, a large part of the recorded energy is caused by seismic waves traveling through the near surface. These are called surface waves, and are supported in elastic solids bounded by the free surface of air above the ground (Yilmaz, 2015). The near surface of the earth is often not a single cohesive, homogeneous rock layer, but a mixture of rock types, with different attributes affecting the propagation of seismic energy. One type of surface wave, Rayleigh-waves, have amplitudes which are heavily influenced by lateral heterogeneities in this near surface layer. Surface waves are also dispersive, meaning that each frequency component of the wave travels at a different velocity (Yilmaz, 2015). Rayleigh-wave signals can contain a large amount of information about the near-surface.

Current methods for inverting from dispersion curves to velocity models assume laterally homogeneous horizontally layered media, which is not representative of the majority of real near surface systems. By analysing the dispersive character of surface waves, it is possible to more accurately estimate near surface properties. In this paper, various near surface models are constructed, with increasingly complex geometries and velocity contrasts. Elastic wave propagation modelling is conducted on these, producing shot records showing the Rayleigh wave dispersion character. Dispersion curves are generated, and compared for different shot locations and models.

SURFACE WAVE BACKGROUND

When elastic solids are bounded by a free surface (of air or water), the solid can support the propagation of waves along this surface, which are referred to as surface waves (Yilmaz, 2015). At non-normal incidence at an interface, an incident compressional (P) wave is partitioned into four components; reflected P-wave and S-wave of SV-type, and transmitted P-wave and SV-type shear wave. When this partitioning occurs at the soil-bedrock interface, the P-P reflected and P-SV waves become trapped in the soil column, and propagate along the free surface as Rayleigh waves with P-SV particle motion (Yilmaz 2015). Rayleigh waves propagate with retrograde elliptical particle motion, as shown in

Figure 1. Particle motion can be seen to be in both the direction of and perpendicular to, the direction of wave propagation.
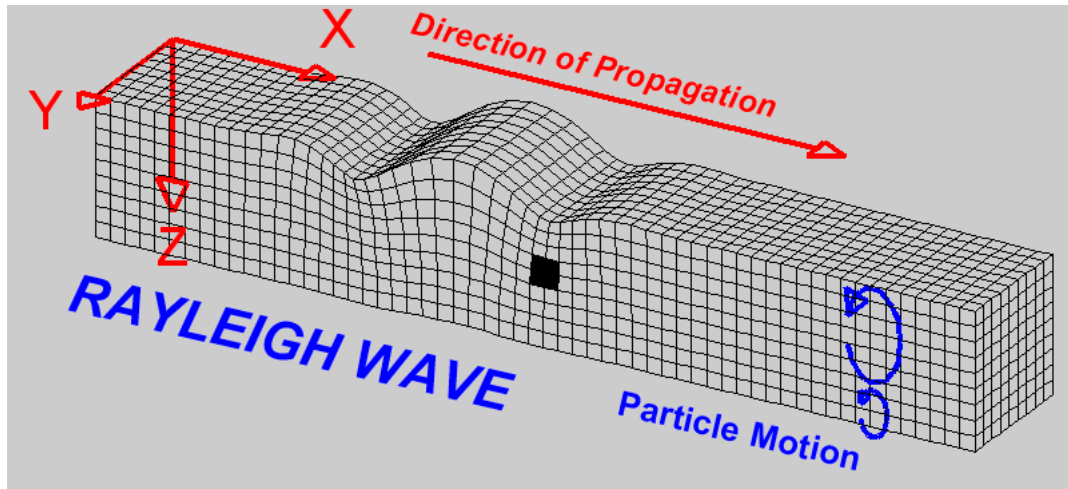

FIG. 1. Rayleigh wave particle motion. (From http://web.ics.purdue.edu/~braile/edumod/waves/Rwave.htm).

Love waves, which have an SH type particle motion that is horizontal and transverse to the propagation direction, arise from an incident SH-wave being reflected as an SH wave which travels along the free surface (Yilmaz, 2015).

Due to the relative distances traveled, as well as the two-dimensional cylindrical character of surface waves compared to the three-dimensional spherical character of body waves, recorded Rayleigh wave amplitudes are greater than body-wave amplitudes (Phillips et al., 2004). As can be seen in Figure 1, Rayleigh wave motion decreases with depth, which is dependent on the frequency of the waves. When a compressional wave source is used (e.g., dynamite, Vibroseis), more than two-thirds of total seismic energy generated takes the form of Rayleigh waves (Richart et al., 1970). Seismic recordings are dominated by these high amplitude events, which is referred to as ground roll. These recorded ground roll waves appear in a "noise-cone" in shot records, which obscures the reflection energy that is of interest in most scenarios. Because of this, in most seismic exploration cases, the ground roll energy is filtered out of the seismic record, and discarded. Recently however, attempts are being made to understand and utilize surface waves. The motivation is two-fold: first, these waves are being recognized as a rich source of information concerning the difficult-to-characterize near surface; and second, filtering and signal rejection is contrary to the philosophy of full waveform inversion, whose aim is to incorporate the wave field as a single, unified entity.

NEAR SURFACE CHARACTERIZATION METHODS

Currently, to support full-waveform inversion, which uses the full recorded wavefield to model the subsurface, near surface attributes such as shear wave velocities, soil properties, and near surface geometries are usually assumed, which likely introduces inaccuracies into the results. The recorded body waves have travelled through the near surface at least twice, at different locations, and as a result will have been affected by these

materials and geometries. Considering that a 2D seismic line or 3D seismic survey may cover many 10s or 100s of km^2 over varied terrain and environments, it is not reasonable to assume that the near surface layers of the earth have the same properties everywhere along these surveys.

Through inversion of ground roll amplitudes and velocity dispersion, these near surface properties may be more accurately modelled. If this inversion could be applied in such a way that the recorded ground roll be used to model the near surface at every point in a survey area, then the subsequent data processing steps could be performed taking into account the attenuative effects of the near surface. This would result in data more representative of the actual wavefield, and as a result, a more accurate interpretation could be made.

Methods exist to characterize the near surface such as spectral analysis of surface waves (SASW), in which a single pair of receivers to study each frequency component of the surface waveforms individually (Nazarin et al., 1983). Multichannel analysis of surface waves (MASW) is a more recent advance, which uses a series of broadband geophones (similar to common midpoint reflection surveys) and a shot from both ends of the array, to measure a swept-frequency source (Park et al., 1999). The repeated shot from the opposite end of the receiver line is used to confirm the results, as well as to detect lateral heterogeneities along the line by comparing the shot gathers, which would be identical for laterally homogeneous horizontally layered media. Due to the acquisition similarities to reflection surveys, and the ease of conducting surveys, the surface wave propagation modelling performed in this project are based on the MASW technique.

The process of MASW after acquisition is to generate a dispersion curve of phase velocity vs frequency for acquired Rayleigh waves, then build initial P-wave, S-wave, and density models for a horizontally layered, laterally homogeneous earth, using estimates for the region of the survey (Yilmaz, 2015). Next, the Rayleigh wave dispersion curve for the model is calculated and compared to the observed dispersion. Using the discrepancy between the modeled and observed curves, the model is adjusted and the process repeated until the difference is minimized (Yilmaz, 2015).
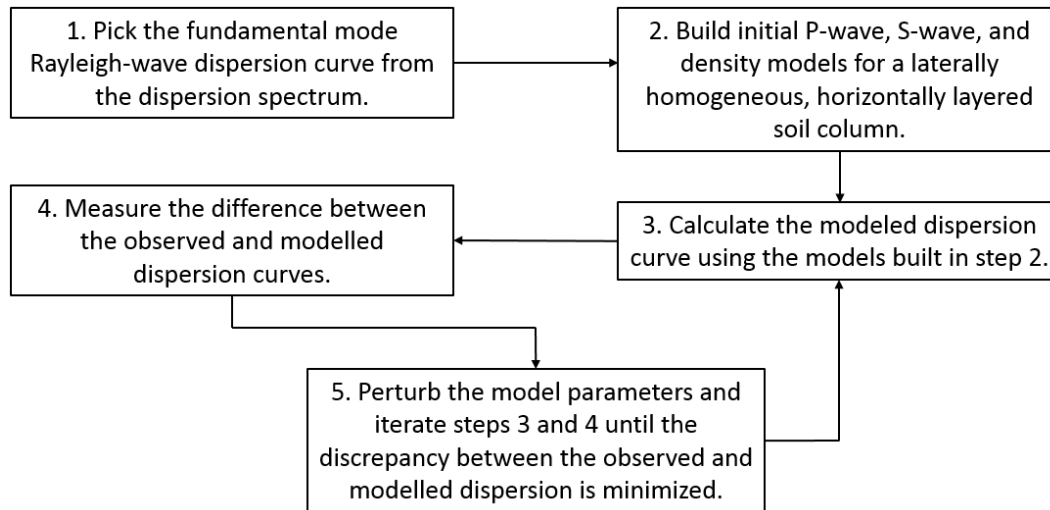
FIG. 2. Workflow for Rayleigh wave inversion, as can be used in MASW. (Adapted from Yilmaz, 2015).

SURFACE WAVE PROPAGATION MODELLING

Modelling software

In this study, all modeling is done using SOFI2D, which is a 2D finite difference seismic modeling engine (Bohlen et al., 2015). Various velocity (Vp and Vs) and density models were built in Matlab, and used as input into SOFI2D (Cova, 2016). The models are 5000m wide by 1000m deep, with the near surface confined to the top 100m of the model. An explosive point source is used in all shot record constructions. In most cases, the source and receivers are placed at 5m depth, within the first near-surface layer. Receivers are placed from 100m to 4900m, with a receiver spacing of 2m. SOFI2D has the ability for the free surface to be toggled on or off, which is useful for observing how ground roll and Rayleigh wave dispersion affects the shot record. The sides and bottom of the model are set as absorbing boundaries, however in some cases artificial reflections from these boundaries still appear. A Fuchs-Muller minimum-phase wavelet with a central frequency of 12 Hz is used. Once SOFI2D has run using the input models, and source and receiver locations, a 2 second shot record is generated with a time sampling rate of 1ms. Shot records can be produced from the vertical receiver component, as well as the radial component if converted waves are of interest.

Dispersion curve generation

Theoretical 1D dispersion curves are generated for elastic, vertically heterogeneous models, using mat_disperse.m (Rix et al., 2003). A 1D model with Vp, Vs, ρ, and layer thicknesses is specified for the function. A vector of frequencies, representative of the source frequencies (e.g. A set of Vibroseis sweep frequencies), and receiver offsets are used to solve the wavefield propagation eigenvalue problem for Rayleigh waves along a free surface, and returns the modal phase velocities, along with the fundamental mode of dispersion.

Shot records generated in SOFI2D are input into DispSpec.m, which performs the following processes (R. Cova, Matlab code, 2016). Dispersion spectra are generated for each shot record through several processes. First, the shot record *d(x, t)* is Fourier transformed over *t* to *d(x, ω)*. This data is then tau-p transformed from *d(x, ω)* to *d(p, τ)*. The discrete tau-*p* transform is described by equation 1 (Turner, 1989)

$$F(\tau, p) = \sum_{i=1}^{n} F(x_i, \tau + px_i) \qquad (1)$$

Where:

n = number of seismic traces used in the transform,

x = horizontal space coordinate or position of the seismic trace,

t = two-way traveltime,

τ = *p*=zero offset intercept,

p = apparent slowness,

f = frequency,

F(x, t) = amplitude at *(x, t)* in the standard seismic section, and

F(τ, p) = amplitude at *(τ, p)* in the tau-*p* domain.

This tau-*p* transform is performed over a range of slowness values, producing tau-p data with twice as many *p* traces as there were x traces. This data is then Fourier transformed over the time variable τ, producing *d(p, ω)*. The phase velocities are then extracted by mapping slowness p to velocity, trace-by-trace, and computing the amplitude spectrum of the tau data (Yilmaz, 2015). Modelled dispersion spectra for the data are finally generated by plotting phase velocity vs frequency *ω*.

Generally, at negative offsets, the dispersion represents negative phase velocities, and the opposite is often true at positive offsets. When there are events which have time dips of opposite polarity to the offset direction, such as in the case of reflection from vertical reflectors, these events will appear on the opposite polarity offset dispersion curve. Theoretical dispersion curves are then overlain on the modelled curve for the same model, and compared, as in step 4 of Fig. 2.

Often, tau-*p* transforms are utilized to filter out coherent noise such as ground roll, especially when this noise is spatially aliased (Turner, 1989). In this paper however, the tau-*p* transform is employed to isolate ground roll and extract near-surface dispersion curves.

MODELS AND DISCUSSION

In order to observe the effects of varying near-surface complexities and geometries on shot records, model complexity will gradually be increased, and shot records with, and without ground roll will be compared, where necessary. The general process of MASW

will be followed (i.e. acquiring shot gathers at multiple points along a survey line, and comparing the dispersion character).

Model 1: Laterally homogeneous, vertical gradient

In Figure 3, a simple, laterally homogeneous, horizontally layered model is illustrated. This model has gradually increasing Vp, Vs, and ρ in the near-surface, with a homogeneous half-space below. The shot record shown in Figure 4 was generated using an absorbing top boundary (FS0), and shows the refracted arrivals from the half-space, as well as the direct P arrivals through the near-surface. Reflections from the near surface layers are obscured by these features. Figure 5 is the shot record generated using a free surface (FS1), and as a result, the Rayleigh waves are now produced. Because there are no lateral velocity variations, and layers with higher velocities are deep enough that Rayleigh waves may not reach them, this model approximates a laterally homogeneous single layer near surface medium. There is little if any dispersion visible in the surface wave arrivals in the shot record, which appear linear. Due to different absorbing boundary conditions, artificial reflections from the sides, and the bottom of the computational volume are visible, and can be seen at the edges and in hyperbolic reflections from 0.7-1s. These false reflections are minimized by increasing the width of absorbing boundaries, and are overshadowed by events resulting from the inclusion of greater complexity in later examples.
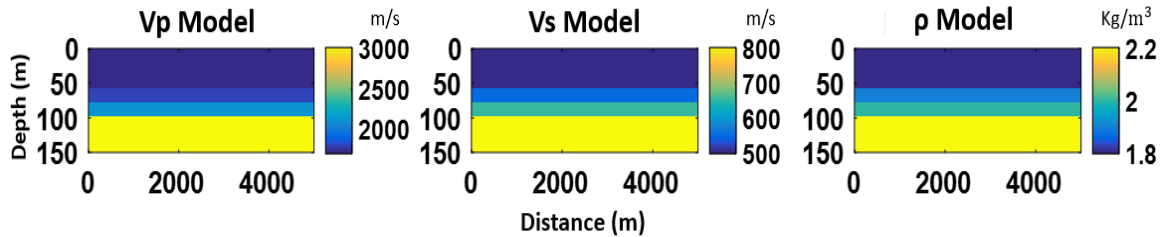

FIG. 3. Velocity and density models of a gradient near surface. The half-space continues to 1000m depth. A 2D smoother has been applied to the models to reduce reflections off layer boundaries.
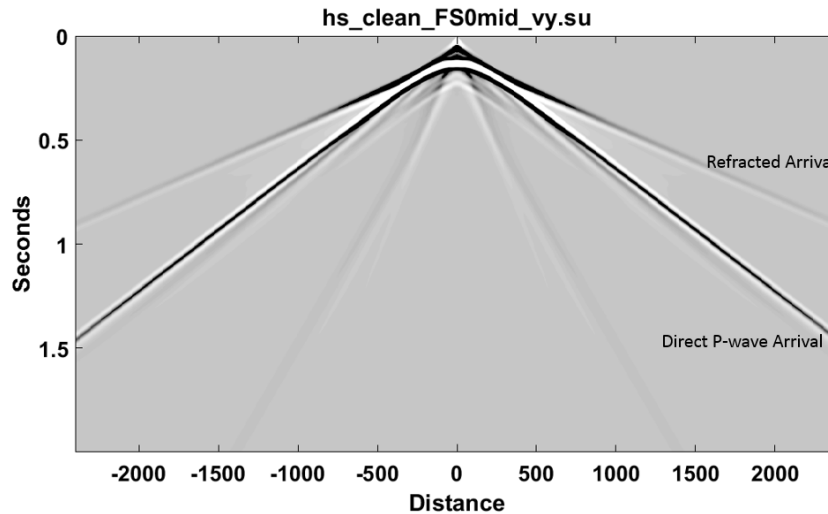

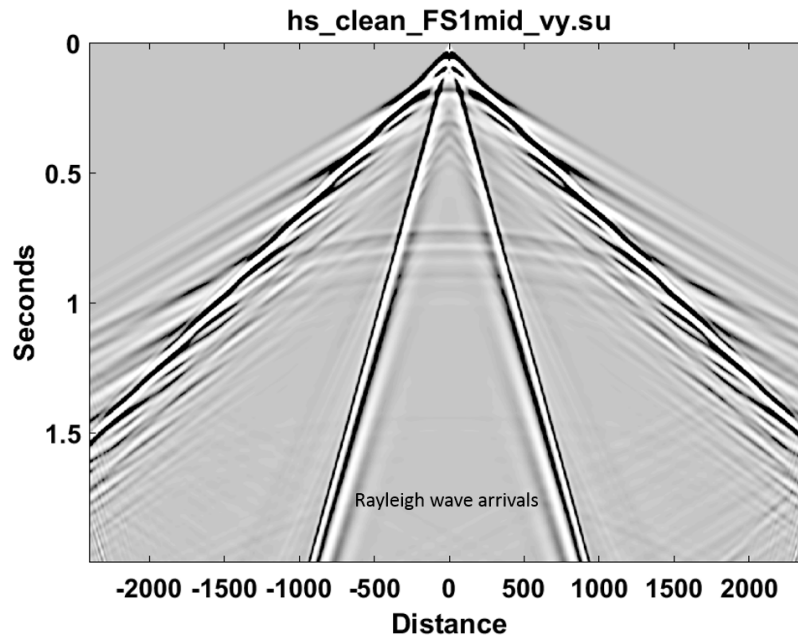FIG. 4. Shot record generated using an absorbing upper boundary. Distance in m from the source.

FIG. 5. Shot record generated using a free surface. Artificial reflections are visible at the edges and in hyperbolic reflections at 0.7-1s.

The modelled dispersion curve for this model is shown in Figure 6, with its theoretical curve overlain. Because of the simplicity of the model, there is a near perfect match between the two curves. There is a small amount of dispersion below 10Hz, which increases towards the lower frequencies.
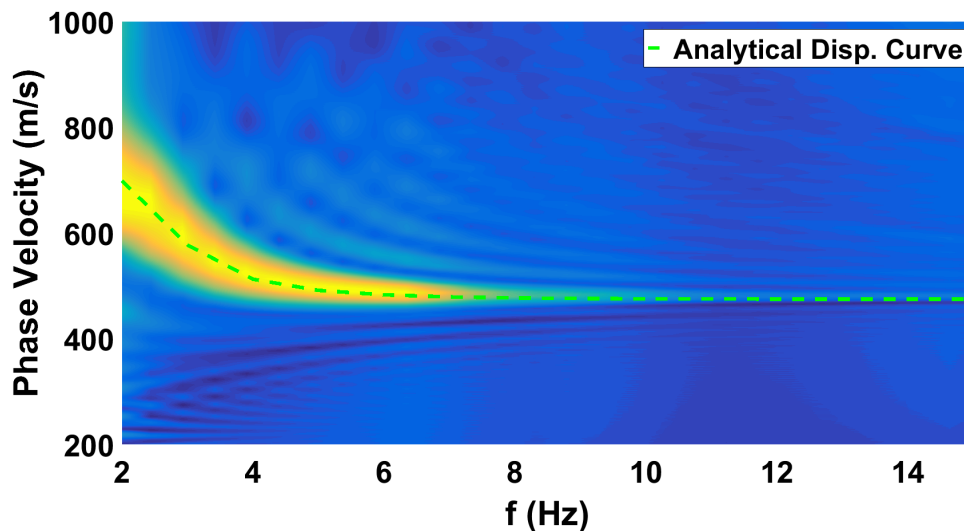

FIG. 6. Dispersion curves for model 1. The background is the modelled dispersion. The overlain dashed line is the analytic velocity model dispersion.

Model 2: Lateral velocity contrast at 2500m

The introduction of lateral heterogeneity results in greater variation of variability in the character of the dispersion. A vertical contact is introduced in the first near-surface layer,

with an increase of ΔVp=100m/s, ΔVs=50m/s, and Δρ=0.1g/cc to the right (Figure 7). The dispersion in Figure 8 is similar on both sides of the source, however, due to the velocity differences on each side, there is time-dip asymmetry on opposing sides, as well as different dispersion character. Due to the thickness of the near surface layer, and the depth of the source (20m), the surface waves are weakly dispersive, but dispersion is more apparent with greater offset. When the source is moved into the left side of the model as in Figure 9, a loss of dispersion is observed. This is caused by the removal of velocity variations near the source, and the model can be approximated by a laterally homogeneous medium. However, because of the vertical velocity contrast in the centre of the model, 300m from the source, there are reflections and transmissions of Rayleigh waves at this contact. These arise both from incident P-waves, as well as incident Rayleigh waves.
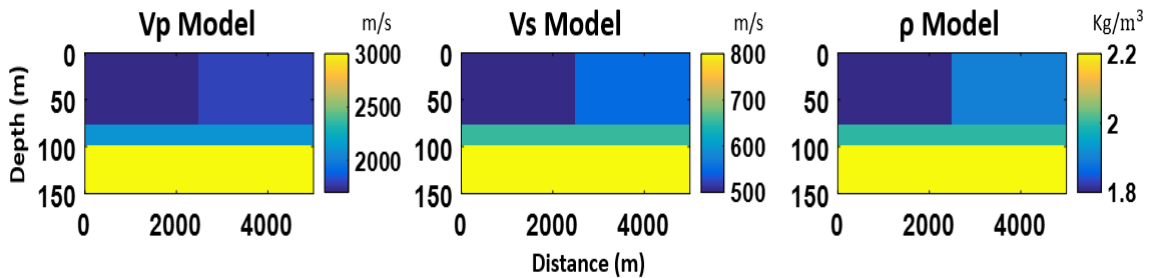

FIG. 7. Velocity and density model of a gradient near surface, with a vertical discontinuity in the centre of the model.
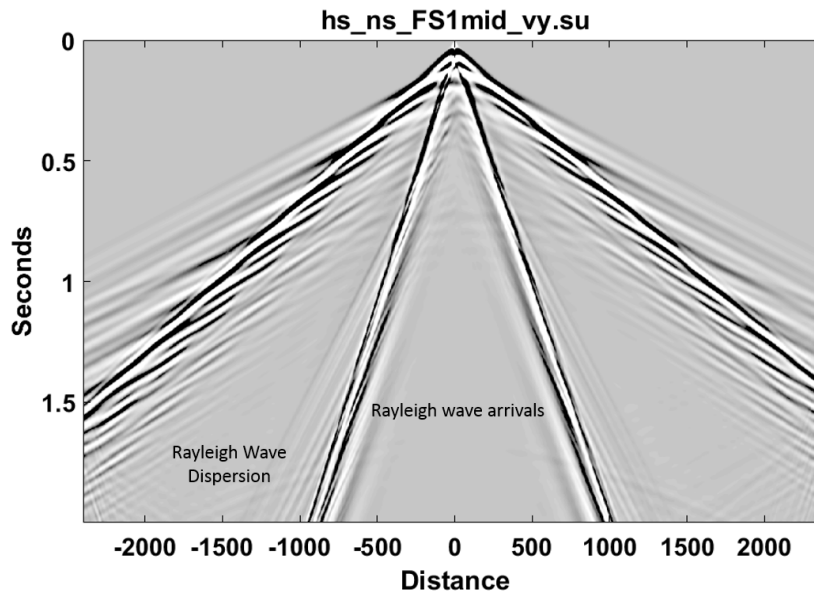

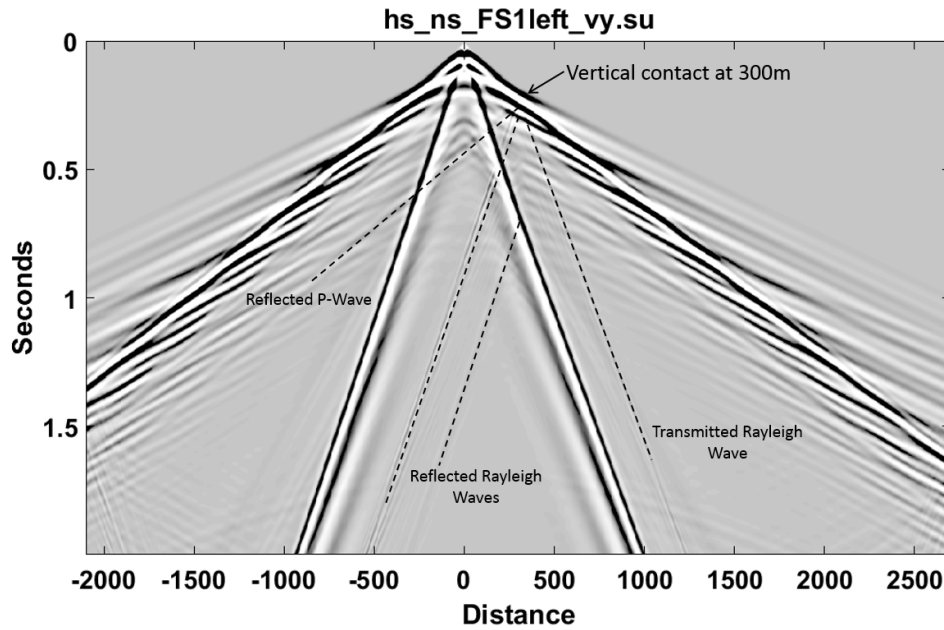FIG. 8. Shot record generated with a shot at x=2500m of model 2. Note asymmetry of direct Rayleigh wave arrivals.

FIG. 9. Shot record with the source at x=2200m of model 2. Note the annotated wave interaction with the contact at 300m offset.

Moving the source and receivers closer to the surface at 5m depth results in greater generation and detection of Rayleigh wave dispersion, as shown in Figure 10A. To compare this to a model with a greater velocity contrast in the near surface, the velocity of the right side of the model is increased by 50m/s. This results in greater dispersion to the right of the contact (>300m offset). This shows that in the above example (Model 1), dispersion is limited by the depth of the source, and detection is limited by the depth of receivers. In Figure 10B, there is also dispersion visible in the Rayleigh-Rayleigh reflected waves, when compared to the smaller velocity contrast in Fig. 10A.
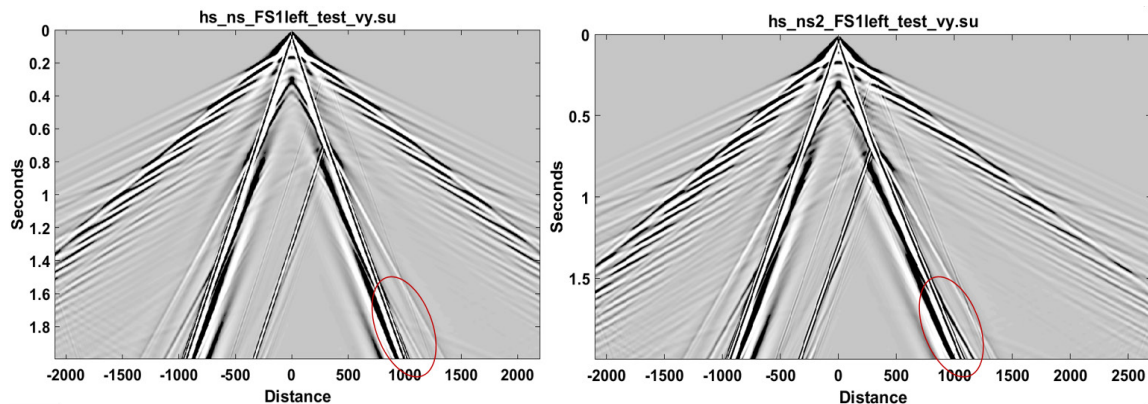

FIG. 10. Left (A): Same model as in Figure 6, with source and receivers at 5m depth. Right (B) Same model geometry, with higher velocity contrast at vertical contact. Slightly more dispersion is visible at 1000m offset of the shot record B (red oval).
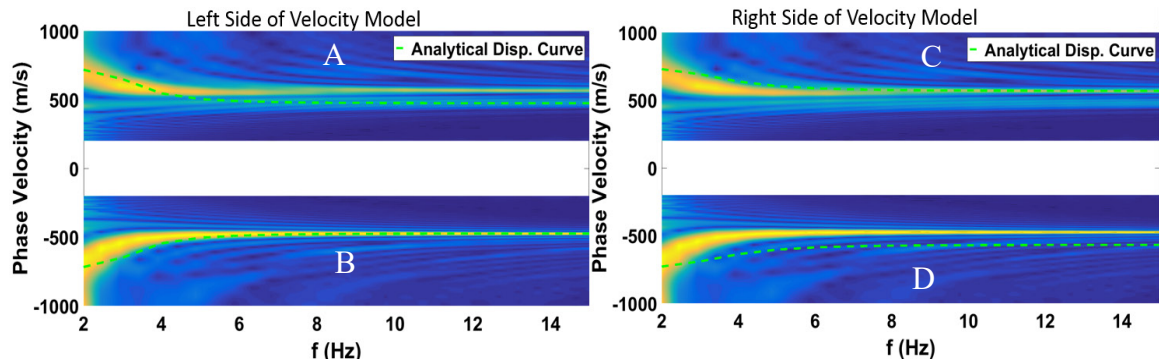
FIG. 11. Dispersion curves for the shot record in Fig. 10B. A) Positive phase velocities. Analytical curve from the left side of the model. B) Negative phase velocities. Analytical curve from the left side of the model. C) Positive phase velocities. Analytical curve from the right side of the model. D) Negative phase velocities. Analytical curve from the right side of the model.

The dispersion curves shown in Fig.11 are generated from the velocity model with a higher contrast at the vertical contact, and the modelled curve is from the shot record with a source in the left side of the model. In most cases positive phase velocities correspond to positive offsets, however, reflections from the discontinuity can have a negative phase velocity at positive offset. The modelled curves are identical in 11A and 11C, but the analytical curves are from opposite sides of the model. In the modelled positive phase velocity dispersion curves (A, C), there appear to be two major fundamental mode curves, which are overlain by the analytical curves. This is due to the inclusion of Rayleigh wave dispersion in the two different velocity "regimes" which lie on either side of the discontinuity. The same effect can be observed in the negative phase velocity dispersion curves, for a source on the opposite side of the model. For a source in the centre of the model (Fig.12), where positive phase velocities represent only positive offsets, there is a very good match between the analytical dispersion and modelled dispersion for positive velocities on the right side of the model, and negative velocities on the left side of the model, as seen in Figure 13.
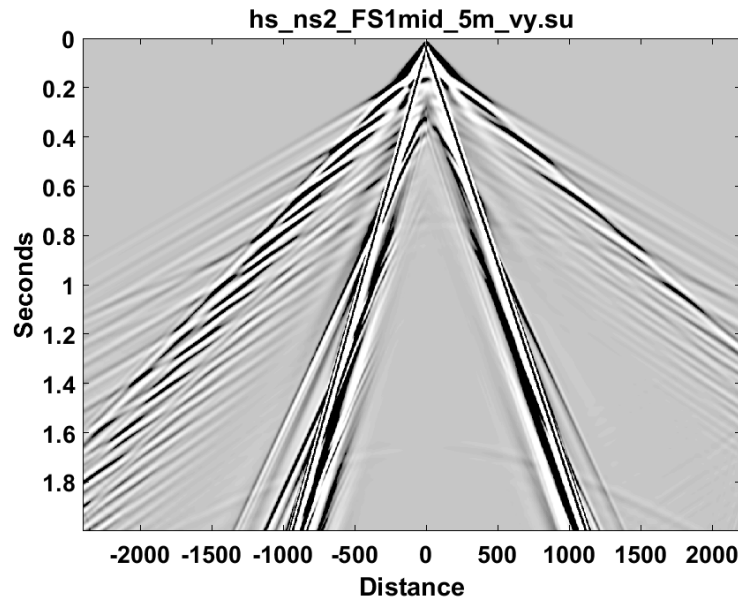
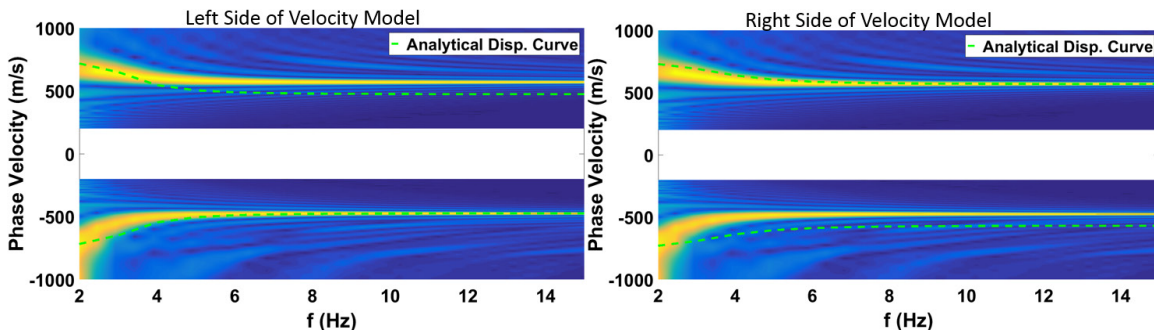FIG. 12. Shot record from the centre of model 2, with the source and receivers at 5m depth.

FIG. 13. Dispersion curves for the shot record in FIG. 12.

Model 3: Multilayer near-surface, with velocity variations, and a vertical discontinuity

The next model to be examined in this report includes a multi-layered near surface, with varying velocities, and a vertical discontinuity in the centre, that is representative of a vertical fault. Compared to Model 1 and 2, the layer 2 and 3 boundaries are closer to the surface, and velocity contrasts are also greater in both vertically and laterally adjacent layers. These differences together should result in greater dispersion.
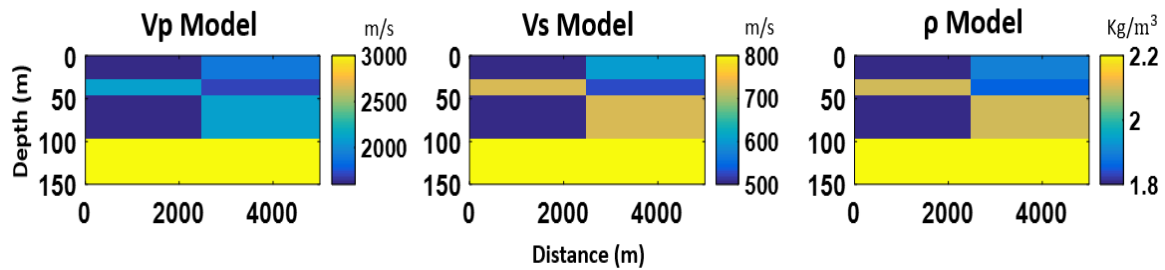

FIG. 14. Velocity and density models of a multi-layered, vertically faulted system.
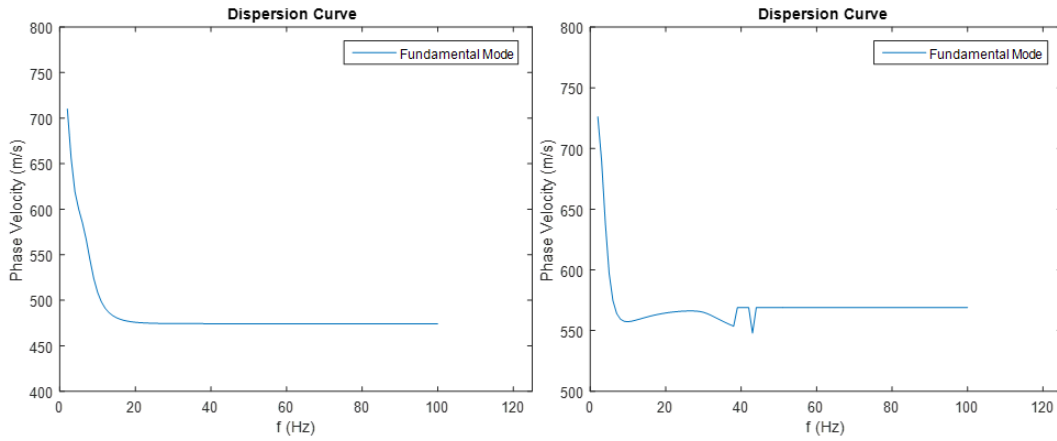
FIG. 15. Analytical dispersion curves for the left side (left) and right side (right) of Model 3.
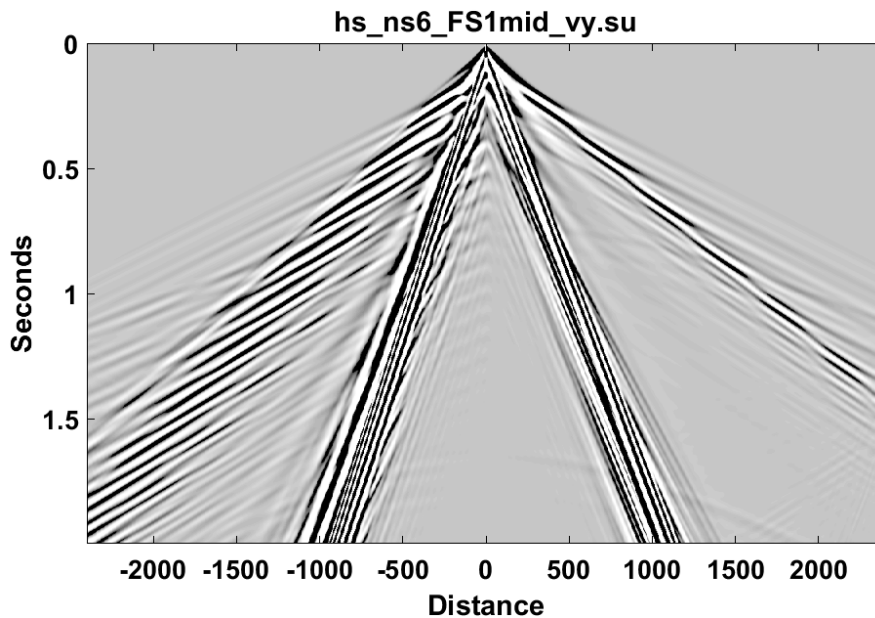

FIG. 16. Shot record for Model 3, with the source at x=2500m, on the discontinuity.

In the shot record from the centre of the model, shown in Figure 16, Rayleigh wave characteristics that are different from the previous examples are clearly visible. Vertical velocity contrasts are more than twice as great (500m/s vs 200m/s) on the left side of the discontinuity, so this is expected. These differences are observed when comparing the opposite polarity dispersion curves for this shot gather, displayed in Figure 17. Of note is the mismatch of the analytic curve to the modelled curve, denoted by *. Because the left side of the velocity model is the only part of the model to influence negative offsets, these curves should match, as they do for Model 2 in Figure 13. This mismatch has consequences for velocity inversion, because the inversion from the modelled curve would generate a velocity model different from the true model.
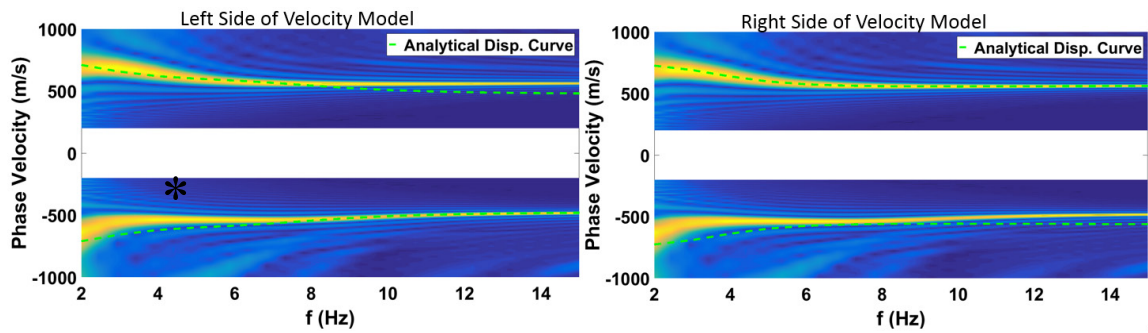
FIG. 17. Dispersion curves for the centre-source shot record of Model 3. Note the poor match at low frequencies of negative phase velocity dispersion curves (*).
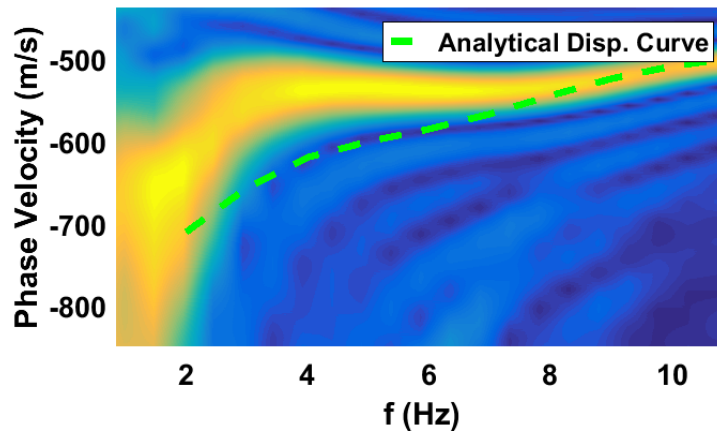

Fig. 18. Zoomed image of the dispersion curve *, showing up to a 100m/s velocity difference.

With synthetic models, there is the ability to isolate dispersion curves for sections of shot gathers over a known model. By isolating dispersion curves for sections of shot gathers representative of a single velocity model, the analytic curve should be matched by the model. Given the results shown in Figures 17 and 18, it appears that for certain cases the modelled dispersion does not match the predicted dispersion. Consequently, errors and/or completely spurious inversion results should be expected to arise.

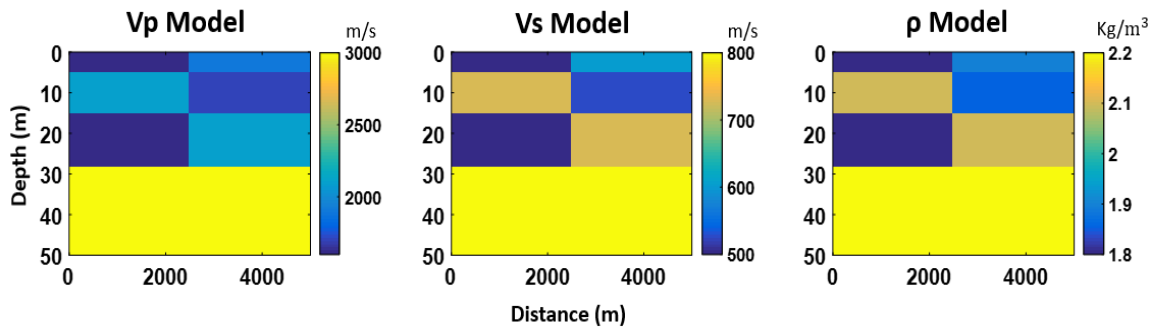**Model 4: Thinner and shallower near-surface layers, same velocities as Model 3**

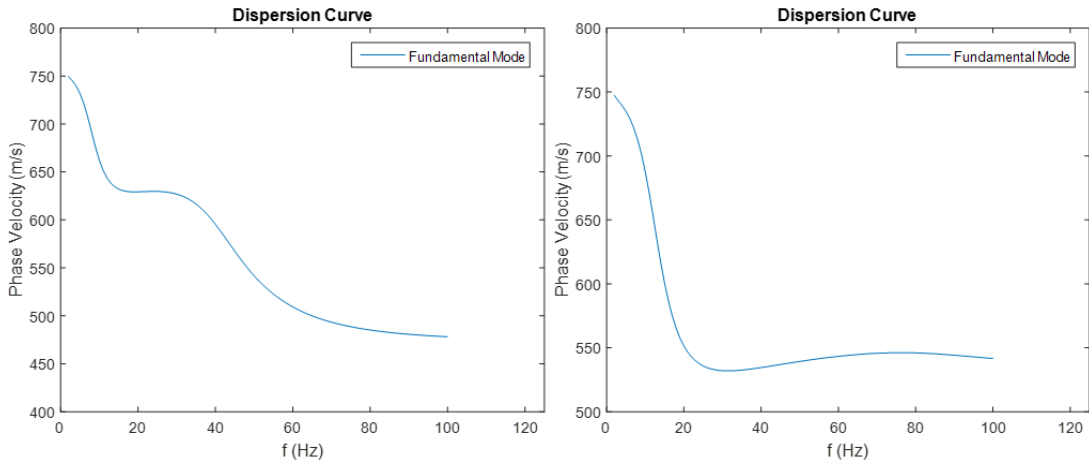FIG. 19. Velocity and density models for Model 4.

FIG. 20. Analytical dispersion curves for the left side (left) and right side (right) of Model 4.

Compared to Model 3, the dispersion curves for Model 4 are more dispersive at higher frequencies, and the different velocity influences are more visible. Because the dispersion is caused by the same velocities in each model, they share the same rough shape, with changes dependent on velocity. Because the layers were deeper in models 2 and 3, only low frequency Rayleigh waves exhibited dispersive behaviour. When the boundaries are closer to the surface as in this example, frequencies up to 100 Hz are dispersive (Figure 20). The dispersion curves for opposite sides of the model are very different, which contributes to the dispersion mismatch seen in Model 3 (Figures 17, 18). This is also observed for this model, shown in Figure 21. The highest "near surface" layer shear wave velocity in this model is 725 m/s, and the half-space shear Vs is 800 m/s. The dispersion curve at low frequency has a phase velocity of 750 m/s, indicating that there are likely Rayleigh waves travelling in the half-space at a depth of 50m. The Rayleigh waves can be seen to be very dispersive in the central shot record (Figure 22), with the three major contributing velocities clearly visible in the different time dips.
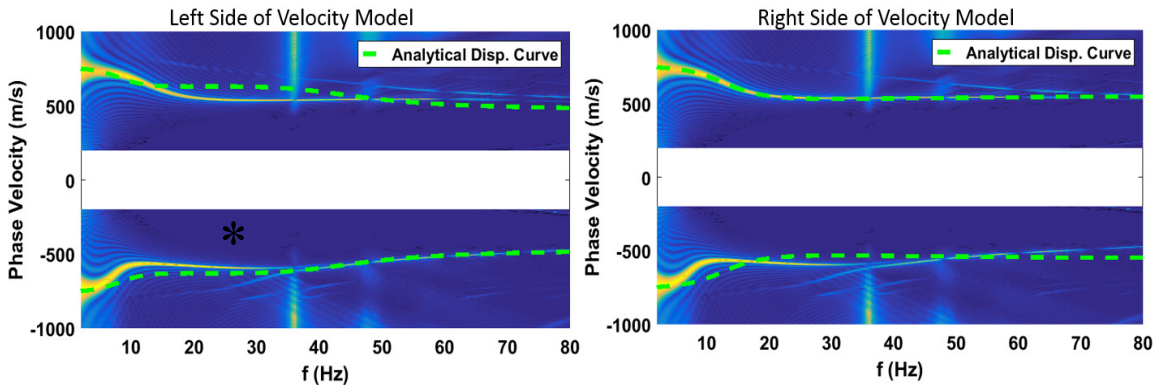

FIG. 21. Dispersion curves for the centre-source shot record of Model 4. Note the poor match at lower frequencies of negative phase velocity dispersion curves (*).
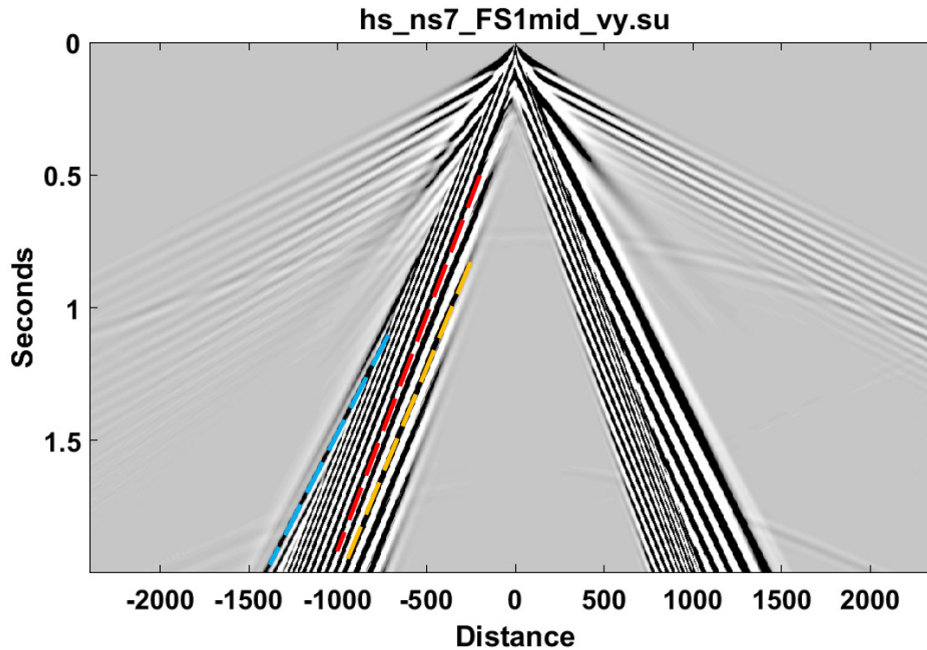
FIG. 22. Shot record for Model 4, with the source at x=2500m, on the discontinuity. The three major contributing velocities are clearly visible in the different time dips (Blue, Red, and Orange).

SUMMARY

In the numerical examples we have examined in this project, Rayleigh waves could be seen to exhibit dispersive behaviour, which changed depending on the model geometries and velocities. As more near surface layers were introduced, more dispersion occurred as a result of additional propagation velocities. As layers moved closer to the free surface, more frequencies were affected, and the different components became more clearly defined in dispersion curves. As layers become thinner, more dispersion occurs as a result of more involvement of additional layers and velocities. With the introduction of sharp lateral velocity changes, we observe reflections and transmissions of Rayleigh waves, including dispersion, from both incident P-waves and Rayleigh waves. By analysing dispersion curves for different shot locations on the survey line, and at different offsets of shot records, lateral boundaries and velocity changes can be detected and located. As seen in Figures 17, 18, and 21, strong lateral velocity variations, coupled with large vertical contrasts, produce a dispersion mismatch between analytic curves and modelled curves. When inverting for near surface velocities and geometries, this mismatch will result in an inaccurate inverted model, which would affect any conclusions drawn from the results, including statics corrections.

LIMITATIONS OF CHARACTERIZATION METHODS

A limitation of MASW for reflection surveys, is that it requires the low frequencies of Rayleigh waves to be measured, often through the use of low-frequency (<10 Hz) geophones, while geophones used for reflection surveys generally have a minimum recording frequency of 10 Hz. However, 10Hz geophones have been shown by Bertram et al. (2010) to have recoverable signal down to 2 Hz at offsets up to 1500m, especially in ground roll. In addition, if Vibroseis is used as the seismic source, sweeps typically begin

at around 6 Hz, meaning low frequencies are not even generated (Harrison, 2011). If the MASW technique and procedure can be adapted for use with existing reflection data, then the possibilities for application to reflection surveys are greatly expanded. In Models 1-3, most of the dispersion is visible in signal below 10 Hz. In Model 4, the <10 Hz frequencies appear to be sampling the half-space, so geophones are adequate for near surface modelling to depths of around 50m.

As stated in the previous section, strong velocity variations in both the x and z direction result in a mismatch between certain components of the dispersion curves, which would result in inaccurate interpretations. This means that the MASW technique could be appropriate for detecting and locating where there are lateral variations, and estimating the scale of these contrasts. However, because of the unaccounted for differences which accrue in dispersion curves, MASW is inappropriate for inverting for near surface velocities in these situations.

CONCLUSIONS

Various near surface velocity models were built, with increasingly complex geometries and greater velocity contrasts between layers. Shot records were generated at multiple points along the model in order to measure Rayleigh wave dispersion, and compare this dispersion at the different shot points. When the wave energy travels through horizontally layered, laterally homogeneous media, the analytic dispersion curve matches the modelled dispersion. When lateral changes are added, and the energy encounters these changes, there is a departure of the modelled dispersion from the analytic curve. This difference increases as velocity contrasts increase, layers thin, and layers approach the free surface. Because of this, MASW is insufficient for characterizing a complex, laterally varying near surface.

Applying the methods outlined in the above report to exploration seismic field data is more difficult. This is due mainly to the limitations in geophone bandwidth and Vibroseis source bandwidth. Without low frequencies, deeper near-surface layers cannot be modelled. Extra processing, including inverse filtering, is required to enhance low frequency signal in existing data (Bertram et al., 2010). Synthetic tests may be run using limited bandwidth data (similar to geophones), or using a swept source beginning at a frequency typical of Vibroseis in order to simulate the application to field data. This would expose any shortcomings of these methods in application to existing seismic data.

This paper provides a background in surface wave propagation modelling and dispersion analysis, to be used in future work improving dispersion curve analysis and adapting reflection seismic data for near-surface studies.

ACKNOWLEDGEMENTS

REFERENCES

Bertram, M.B., and Margrave, G.F., 2010, Recovery of low frequency data from 10Hz geophones, CREWES Research Reports, Volume **22**.

Bohlen, T., D. De Nil, D. Kohn and Jetschny S., 2015, - SOFI2D - seismic modeling with finite differences 2D - elastic and viscoelastic version. Karlsruhe Institute of Technology.

Harrison, C.B, G.F. Margrave, M. Lamoureux, A. Siewart, and Barrett, A., 2011, Harmonic decomposition of a Vibroseis sweep using Gabor analysis, CREWES Research Reports, Volume **23**.

Nazarian, S. K.H. Stokoe, and Hudson, W.R., 1983, Use of spectral analysis of surface waves method for determination of moduli and thicknesses of pavement systems, *Transportation Res. Record*, **930**, 38-45.

Park, C.B, R.D. Miller, and Xia, J., 1999, Multichannel analysis of surface waves, *Geophysics*, **64**(3), 800-808.

Perez Solano, C.A., D. Donno, and Chauris, H., 2014, Alternative waveform inversion for surface wave analysis in 2-D media, *Geophysical Journal International*, **198**, 1359-1372.

Phillips, C., G. Cascante, and Hutchinson, D.J., 2004, Evaluation of horizontal homogeneity of geomaterials with the distance analysis of surface waves, *Canadian Geotechnical Journal*, **41**, 212-226.

Richart, F.E., J.R. Hall, and Woods, R.D., 1970, Vibrations of soils and foundations, Prentice-Hall, Inc.

Rix, J., and Lai, C.G., 2003, mat_disperse.m Matlab code, used under GNU General Public License, Free Software Foundation.

Yilmaz, O. 2015, Engineering seismology with applications to geotechnical engineering, Society of Exploration Geophysicists.